Magnetic inhomogeneity in charge-ordered $La_{1.885}Sr_{0.115}CuO_4$ studied by NMR

A. Arsenault,[1] T. Imai,[1] P. M. Singer,[2] K. M. Suzuki,[3] and M. Fujita[3]
[1]*Department of Physics and Astronomy, McMaster University, Hamilton, Ontario, Canada L8S4M1*
[2]*Department of Chemical and Biomolecular Engineering, Rice University, 6100 Main Street, Houston, Texas 77005-1892, USA*
[3]*Institute for Materials Research, Tohoku University, Sendai 980-8577, Japan*

(Received 29 December 2018; revised manuscript received 2 March 2020; accepted 5 March 2020; published 11 May 2020)

We report the inverse Laplace transform analysis of the ^{139}La nuclear spin-lattice relaxation rate $1/T_1$ (ILTT$_1$ analysis) in charge-ordered $La_{1.885}Sr_{0.115}CuO_4$ ($T_{charge} \simeq 80$ K, $T_c \simeq T_{spin}^{neutron} = 30$ K), and shed light on its magnetic inhomogeneity. We *deduce* the probability density function $P(1/T_1)$ of the distributed $1/T_1$ (i.e., the histogram of distributed $1/T_1$) by taking the inverse Laplace transform of the experimentally observed nuclear magnetization recovery curve $M(t)$. We demonstrate that spin freezing sets in *in some domains* precisely below the onset of charge order at T_{charge}, but their volume fraction grows only gradually toward T_c. Nearly a half of the sample volume exhibits properties expected for canonical high-T_c cuprates without charge order even near T_c. Our findings explain why charge order does not suppress T_c of $La_{1.885}Sr_{0.115}CuO_4$ as significantly as in $La_{1.875}Ba_{0.125}CuO_4$.

DOI: 10.1103/PhysRevB.101.184505

I. INTRODUCTION

Recent advances in x-ray diffraction techniques led to successful detection of charge-order Bragg peaks in $La_{2-x}Sr_xCuO_4$ ($x \simeq 1/8$) below $T_{charge} \simeq 80$ K [1–3]. The confirmation finally settled the old controversy stemming from our earlier reports that the unusual NMR anomalies identified at the charge order transition of $La_{1.48}Nd_{0.4}Sr_{0.12}CuO_4$ are shared with $La_{1.88}Sr_{0.12}CuO_4$, $La_{1.875}Ba_{0.125}CuO_4$, and $La_{1.68}Eu_{0.2}Sr_{0.12}CuO_4$, and hence all of these La214-type cuprates undergo a charge-order transition at a comparable temperature [4–7]. In fact, the charge-order phenomenon turns out to be more ubiquitous across different classes of high-T_c cuprates [8–18], contrary to the belief held by many researchers two decades ago that charge order was merely an odd by-product of the structural transition into the low-temperature tetragonal (LTT) phase of $La_{1.48}Nd_{0.4}Sr_{0.12}CuO_4$.

The fundamental difficulty encountered in the experimental investigation of charge order in the La214 family is that the amplitude of the charge density modulation is extremely small. For the NMR investigation, there is an additional challenge: Charge order triggers glassy spin freezing *within charge-ordered domains* of the La214 family [19] and begins to *locally* enhance the NMR relaxation rates with a wide distribution [4–6]. Since ^{63}Cu NMR relaxation rates in high T_c cuprates are generally enhanced by the Cu-Cu superexchange interaction even without charge order, mild enhancement of the low-frequency Cu spin fluctuations (and hence the NMR relaxation rates) by a factor of $\simeq$3 makes the ^{63}Cu NMR signal detection difficult, i.e., signal intensity wipe out [4–6,20,21]. In fact, our recent single-crystal ^{63}Cu NMR measurements on $La_{1.885}Sr_{0.115}CuO_4$ [20] confirmed that canonically behaving ^{63}Cu signals are gradually wiped out below T_{charge}. The lost spectral weight is gradually transferred to a broad, winglike signal with extremely fast NMR relaxation rates. The latter originates from charge-ordered domains with enhanced spin correlations and can be detected down to $\simeq$30 K only with extremely fast separation time $\tau \simeq 2$ μs between the 90- and 180-deg radio frequency pulses. We note that such an experimental condition was not technically feasible in the 1990s.

In contrast, ^{139}La NMR signals are observable in the entire temperature range, because hyperfine couplings between ^{139}La nuclear spins and Cu electron spins are weaker, and hence the ^{139}La NMR relaxation rates are much slower. The downside of the ^{139}La NMR study is that the spin-lattice relaxation rate $1/T_1$ in the charge-ordered state has a broad distribution due to the glassy nature of spin freezing below T_{charge}. The NMR community did not have an effective tool to deal with such a distribution to make concrete statements about $1/T_1$ results. As mentioned above, two different types of ^{63}Cu NMR signals are observed for $La_{1.885}Sr_{0.115}CuO_4$ with different $1/T_1$ [20], indicating the presence of two different types of domains, but the corresponding ^{139}La NMR signals are superposed [22]. Then how shall we discern their $1/T_1$? We recently tried to circumvent the difficulty by assuming that two distinct components exist in the ^{139}La nuclear spin-lattice relaxation recovery curve $M(t)$ [22]. The relative fractions of the fast and slow $1/T_1$ contributions in $M(t)$ agree reasonably well with the relative intensities of the two different ^{63}Cu NMR signals, but the double component fit is based on an assumption.

In this paper, we re-examine the $1/T_1$ process at the ^{139}La sites based on the inverse Laplace transform (ILT) analysis of the experimentally observed T_1 recovery curve $M(t)$ (dubbed ILTT$_1$ analysis hereafter) [23–26]. The ILT allows us to *deduce* the probability density distribution $P(1/T_1)$ for distributed $1/T_1$ (i.e., the histogram of $1/T_1$ distribution)

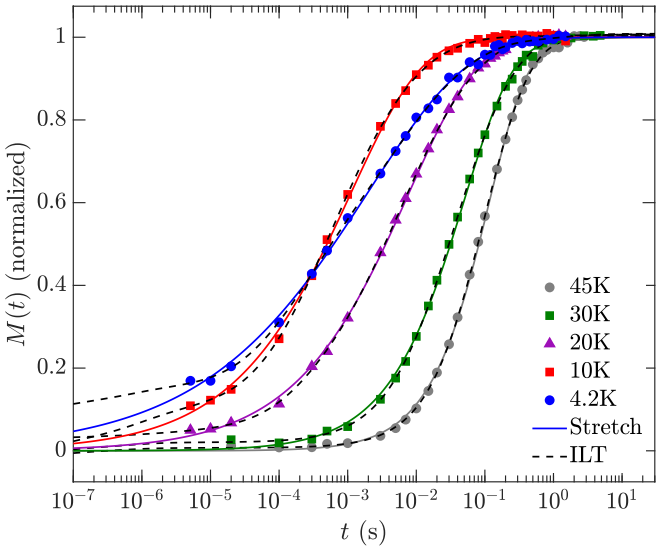

FIG. 1. ^{139}La NMR recovery curves $M(t)$ at representative temperatures, normalized by $(M(t) - M_0)/A + 1$, where M_0 and A are parameters from the best fits (solid curves) to the stretched exponential form in Eq. (2). Also shown are best fits to the ILT (dashed black lines) using Eq. (3). Notice that the broad distribution in $P(1/T_1)$ below 20 K leads to poor stretched exponential fits, while the ILT yields good fits.

without making any assumptions on the functional form of $M(t)$. If $1/T_1$ is distributed around one value, $P(1/T_1)$ will have one peak. But $P(1/T_1)$ will exhibit a double-peak structure if $1/T_1$ is distributed about two distinct values, as we demonstrated elsewhere based on a simple example (see Fig. 1 of Ref. [25]). In what follows, we show that $1/T_1$ in charge-ordered $La_{1.885}Sr_{0.115}CuO_4$ indeed develops an asymmetric distribution, indicative of the presence of two different types of domains below T_{charge}. We establish that charge order does not uniformly affect the entire CuO_2 planes, and the volume fraction of the charge-ordered domains grows only progressively toward $T_c = 30$ K.

II. EXPERIMENTAL

We grew the $La_{1.885}Sr_{0.115}CuO_4$ single crystal at Tohoku using the traveling solvent floating zone method [27]. We annealed the crystal in flowing oxygen gas atmosphere at 900 °C for 72 h. The crystal used for the present study is the same piece as in our previous studies [20,22] and has the approximate dimensions of 3 × 3 × 1 mm. We determined the superconducting critical temperature $T_c = 30$ K based on the magnetization measured with a superconducting quantum interference device (SQUID). $La_{1.885}Sr_{0.115}CuO_4$ is known to enter the spin-ordered phase below $T_{spin}^{neutron} \simeq T_c$ at the fast measurement time scale of elastic neutron scattering [27], and the residual spin fluctuations become static at the slower measurement timescale of muon Spin Resonance (μSR) below $T_{spin}^{\mu SR} \simeq 15$ K [28,29].

We conducted all the ^{139}La NMR measurements at McMaster based on standard pulsed NMR techniques in an external magnetic field of 9 T applied along the crystal c axis. See Ref. [22] for representative NMR lineshapes for the $I_z = +1/2$ to $-1/2$ central transition. Note that the NMR linewidth is dominated by the second-order quadrupole interaction down to T_{charge}, where a mild line broadening sets in due to magnetic effects. For the c-axis field geometry, NMR line shape is not affected by the simultaneous superconducting and spin ordering at $T_c \simeq T_{spin}^{neutron} \simeq 30$ K.

III. RESULTS AND DISCUSSIONS

In the case of nuclear spin $I = 7/2$ at ^{139}La sites, the nuclear spin-lattice relaxation process after the inversion results in the recovery of the nuclear magnetization $M(t)$ following

$$M(t) = M_0 - A\sum_{k=1}^{4} p_k e^{-q_k t/T_1}, \tag{1}$$

where M_0 is the maximum spin echo intensity, and A represents the degree of inversion. The coefficients $\{p_k\} = \{1/84, 3/44, 75/364, 1225/1716\}$ (where $\sum_{k=1}^{4} p_k = 1$) and $\{q_k\} = \{1, 6, 15, 28\}$ are theoretically calculated and fixed for each of the four normal modes in the recovery of nuclear spin $I = 7/2$ [30,31]. When $1/T_1$ has a distribution, it has become a common practice in the literature to stretch each of the four exponentials with a common stretched exponent β, as

$$M(t) = M_0 - A\sum_{k=1}^{4} p_k e^{-(q_k t/T_1^{str})^{\beta}}, \tag{2}$$

where $1/T_1^{str}$ is the stretched fit result of $1/T_1$. In the case of single exponential recovery function expected for NMR measurements of $I = 1/2$ or nuclear quadrupole resonance (NQR) measurements of $I = 3/2$, there are justifications for stretching the exponential function [32–35]. But for the multiexponential recovery function for $I = 7/2$, using the same β for all four normal modes in Eq. (2) should be considered phenomenological. Nonetheless, as we will show below, our ILTT_1 analysis found that this common practice works fairly well for the purpose of estimating the *average value* of $1/T_1$, at least in the present and some other cases [25,26].

The inverse Laplace transform (ILT) [35] consists of fitting the measured recovery curve $M(t)$ to a sum of exponentials with decay rate $1/T_{1j}$ and the probability density $P(1/T_{1j}) \geqslant 0$ [24,25]. More specifically, in the present case of $I = 7/2$, the ILT consists of inverting the following multiexponential equation of four normal modes for $P(1/T_{1j})$:

$$M(t) = \sum_{j=1}^{m}\sum_{k=1}^{4}[1 - 2p_k e^{-q_k t/T_{1j}}]P(1/T_{1j}), \tag{3}$$

where the summation $\sum_j P(1/T_{1j}) = M_0$ is the saturated value of the magnetization at very long delay times $t \gg T_1$. For mathematical clarity, we assumed that inversion is perfect in Eq. (3).

Given the broad distribution in $P(1/T_{1j})$ at low temperatures in the present case, we selected $m = 150$ bins equally spaced on a logarithmic scale ranging from $10^{-2}\,s^{-1} \leqslant 1/T_{1j} \leqslant 10^5\,s^{-1}$. The large upper bound used for $1/T_{1j}$ also allow us to account for imperfect inversion [25]. The probability density is normalized to $\sum_j P(1/T_{1j})\Delta_P = 1$, where $\Delta_P =$

$\log_{10}(1/T_{1j+1}) - \log_{10}(1/T_{1j}) = 0.04698$ is the logarithmic bin spacing. With this normalization, $P(1/T_{1j})$ represents the probability density for the relaxation rate to have the particular value $1/T_{1j}$. Inverting for $P(1/T_{1j})$ in Eq. (3) is an ill-conditioned problem, and therefore requires Tikhonov regularization (i.e., a smoothing factor α) [36–38] or other techniques [39,40] for a solution.

We provide a brief explanation of the ILT technique in the Appendix, and we also discuss the concept of resolution and uncertainties in $P(1/T_1)$. We refer readers to Supplemental Materials [41] of Ref. [25] for additional mathematical background, the optimization procedures of the ILT, and how we treat the case of imperfect inversion in Eq. (3).

In Fig. 1, we present a few examples of the $M(t)$ measured for the $I_z = +1/2 \leftrightarrow -1/2$ central transition based on an inversion recovery technique, with the aforementioned stretched fit with Eq. (2) and the ILT fit in Eq. (3). We used the pulse separation time $\tau = 30\ \mu$s between the 90- and 180-deg radio-frequency pulses, and spin echo recycling time up to $t_{\rm recycle} \simeq 10$ s to ensure that we do not overlook the longest components of the distributed $1/T_1$ in $P(1/T_1)$. The typical 90-deg (180-deg) pulse width is 2.5 μs (5 μs). We averaged the spin echo signals iteratively up to 120 times, with the overall acquisition time of $M(t)$ up to ≈ 12 h. We note that the relaxation rate $1/T_1^{str}$ determined from the stretched exponential fit hardly changes even if one uses $t_{\rm recycle}$ that is somewhat too short, but $P(1/T_1)$ would lose longer components. In addition, the "resolution" of the ILT curve $P(1/T_1)$ depends on the signal-to-noise ratio (SNR) of $M(t)$, as discussed briefly in the Appendix and in detail in the Supplementary Materials of Ref. [25]. Accordingly, the noise level in the $M(t)$ curve should be kept as small as possible (ideally, $\simeq$0.1%).

In Fig. 2, we summarize the $P(1/T_1)$ curves at representative temperatures. The filled bullet superposed on each curve marks $P(1/T_1^{lm})$ at the log-mean value of the relaxation rate, $1/T_1^{lm}$. $1/T_1^{lm}$ is the center of gravity of $1/T_1$ distribution on a logarithmic scale, and represents the spatially averaged value of $1/T_1$ in the entire sample. For example, the red $P(1/T_1)$ curve deduced at 45 K indicates that $1/T_1$ is distributed between $\simeq$0.09 s^{-1} and $\simeq$1.6 s^{-1}; the most likely value is $1/T_1 \simeq 0.29$ s^{-1} as determined by the location of the peak marked by the red upward arrow; the average value $1/T_1^{lm} \simeq 0.37$ s^{-1} (red filled bullet) is not at the peak, because $P(1/T_1)$ is asymmetrical.

We also summarize $P(1/T_1)$ as a color contour map in Fig. 3. The additional relaxation processes caused by the slow fluctuations of the electric field gradient (EFG) enhance $1/T_1$ near the structural phase transition from the high-temperature tetragonal (HTT) to the low-temperature orthorhombic (LTO) structure at $T_{\rm HTT-LTO} \simeq 255$ K, accompanied by the broader distribution and a split off peak at $1/T_1 \simeq 10^2$ s^{-1}. We found analogous results near the structural phase transitions of $La_{1.875}Ba_{0.125}CuO_4$ [25]. Otherwise, the distribution of $P(1/T_1)$ is narrow from 295 K down to $T_{\rm charge}$, and the log-mean value $1/T_1^{lm}$ decreases smoothly.

In Fig. 4(a), we summarize the temperature dependence of $1/T_1^{lm}$ (blue filled bullets) and compare with $1/T_1^{str}$ estimated from the conventional stretched fit of $M(t)$ (red diamonds) [22]. $1/T_1^{str}$ agrees with the log-mean value $1/T_1^{lm}$, and hence the former is a good approximation of the latter. Also summarized in Fig. 4(b) is the stretched exponent β obtained from the stretched fit of $M(t)$ in Eq. (2) [22]. β shows anticorrelation with the log-standard deviation σ_e calculated for the distribution, $P(1/T_1)$. That is, when β decreases from 1 due to

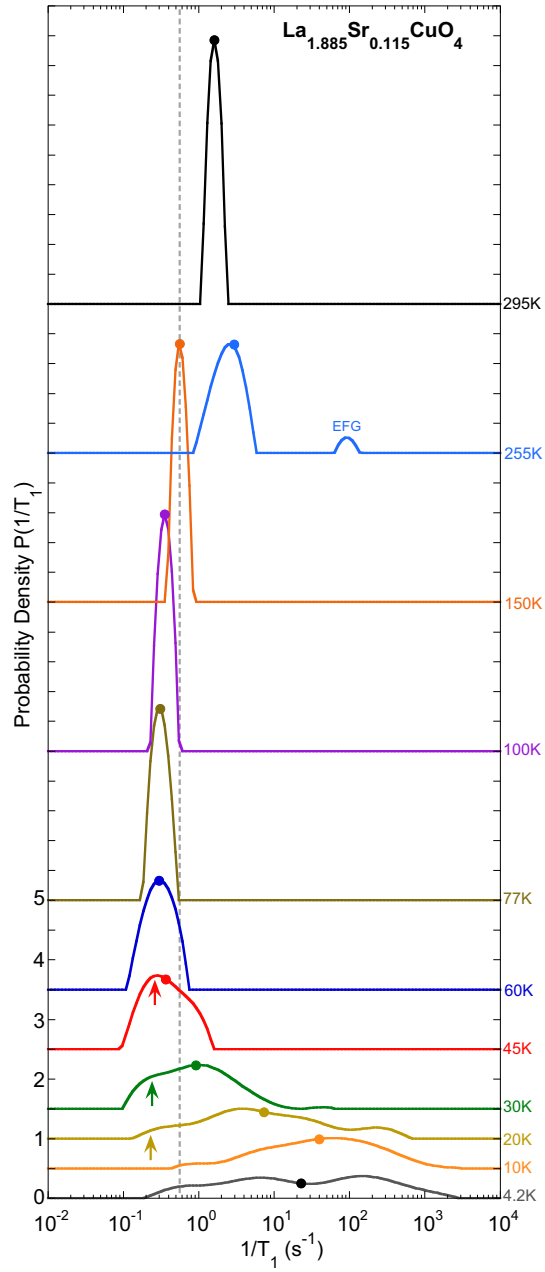

FIG. 2. Representative results of the probability density $P(1/T_1)$ deduced with ILT by numerically inverting experimentally observed $M(t)$. For clarity, the origin is shifted vertically above 4.2 K. Filled bullets mark $P(1/T_1^{lm})$ at the log-mean value of $1/T_1^{lm}$, which is the center of gravity of the $P(1/T_1)$ curve on a log scale. A small split-off peak marked as EFG at 255 K arises from the slow fluctuations of the EFG at the high-temperature tetragonal to low-temperature orthorhombic structural phase transition [25]. Upward arrows show the peak (45 K) and shoulder (30 K and 20 K) overlooked by the conventional analysis based on stretched exponential fit. Dashed vertical line is the cut off at $1/T_1 = 0.55$ s^{-1} for the canonical superconducting domains; see the main text for details.

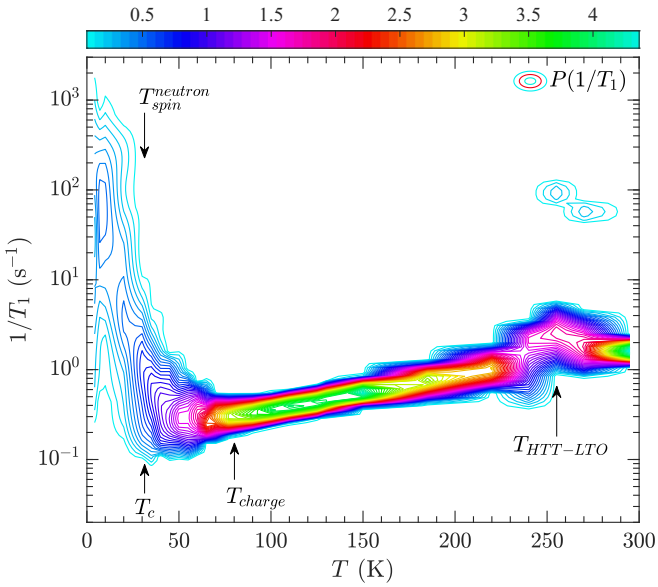

FIG. 3. Contour map of $P(1/T_1)$ (probability density) generated from ILT, using 64 contours. Color bar scale is shown at the top of the figure.

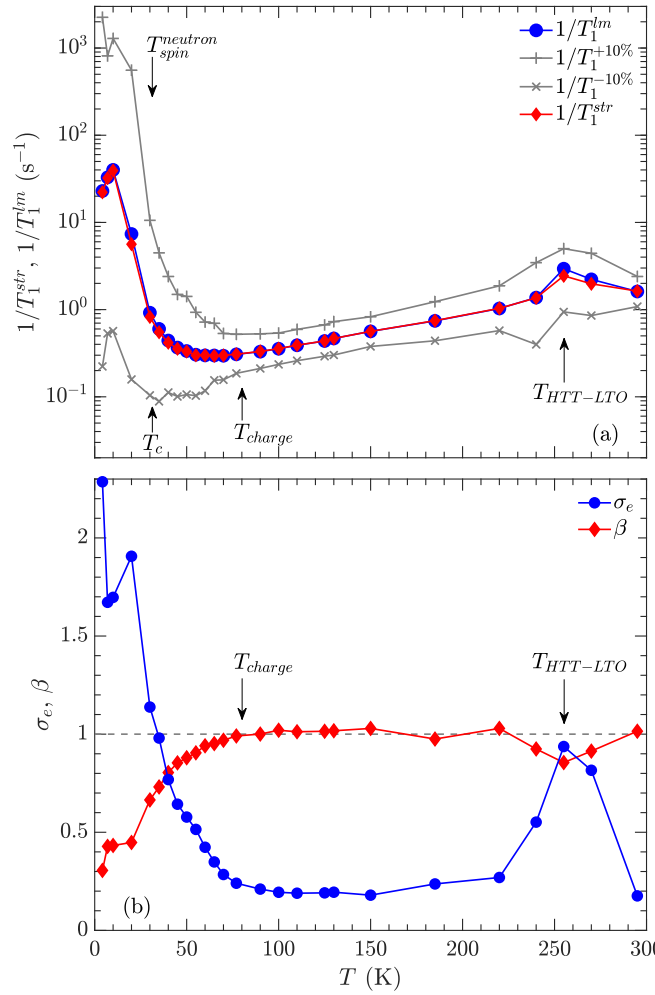

FIG. 4. (a) Blue filled bullets: $1/T_1^{lm}$, the log-mean value of the distributed $1/T_1$ estimated from $P(1/T_1)$. Gray pluses (+): $1/T_1^{+10\%}$, the top 10% value of the distributed $1/T_1$. Gray crosses (×): $1/T_1^{-10\%}$, the bottom 10% value of the distributed $1/T_1$. Notice that $1/T_1^{+10\%}$ begins to grow as soon as charge order sets in, but $1/T_1^{-10\%}$ continues to slow down toward the simultaneous onset of superconductivity and magnetic order at $T_c \simeq T_{\rm spin}^{\rm neutron} \simeq 30$ K. Also shown is $1/T_1^{str}$ (red diamonds), obtained from the single component stretched fit of $M(t)$ [22]. $1/T_1^{str}$ turns out to be a good approximation of $1/T_1^{lm}$, but fails to capture other important features in the distribution of $1/T_1$. (b) The standard deviation σ_e of $P(1/T_1)$, in comparison to the stretched exponent β for the stretched fit. Notice the clear signature of anticorrelation.

the distribution of $1/T_1$, σ_e grows. This makes sense, because deviation from $\beta = 1$ signals the extent of distribution in $1/T_1$, whereas σ_e is the direct measure of the width of the distribution in $1/T_1$. These findings in Fig. 4 establish that the ILT results of $1/T_1^{lm}$ and σ_e can provide us with the equivalent information as $1/T_1^{str}$ and β obtained from the conventional stretched fit analysis. However, all other information about $P(1/T_1)$ is lost when using the stretched fit with Eq. (2).

A major thrust of the ILT$_1$ analysis is that we can go one more major step beyond elucidating the *average behavior* and examine *exactly how* $1/T_1$ *distributes about the average value* $1/T_1^{lm}$. Let us now closely examine how charge order affects the distribution of the local magnetic environment. First, note that $P(1/T_1)$ has a single narrow peak with minimal distributions between 295 K and $T_{\rm charge}$ except near $T_{\rm HTT-LTO}$. This is consistent with the fact that the conventional stretched fit returns $\beta \simeq 1$ in this temperature range, implying that there is little distribution in $1/T_1$. The finite width of $P(1/T_1)$ above $T_{\rm charge}$ is set primarily by the resolution of the ILT [25]. Also note that $1/T_1^{lm}$ is located at the peak of $P(1/T_1)$ down to $T_{\rm charge}$, because the distribution of $P(1/T_1)$ is symmetrical on a logarithmic scale, except near $T_{\rm HTT-LTO}$.

The situation completely changes below $T_{\rm charge} \simeq 80$ K, as clearly shown by the closeup view of $P(1/T_1)$ in Fig. 5. $P(1/T_1)$ begins to broaden asymmetrically by extending a tail toward larger values of $1/T_1$ due to glassy spin freezing. At 50 and 45 K, the main peak of $P(1/T_1)$ is still shifting toward the smaller values of $1/T_1$, and the residue of the peak is recognizable as a shoulder at $1/T_1 \simeq 0.25$ s^{-1} down to $\simeq 20$ K. These ILT results indicate that $1/T_1$ at a considerable fraction of ^{139}La sites is still decreasing below $T_{\rm charge}$, although the sample averaged $1/T_1^{lm}$ (filled bullets) is pulled toward the larger value of $1/T_1$ due to the growing tail toward larger $1/T_1$.

To quantify these observations, in Fig. 4(a) we plot the top 10% value $1/T_1^{+10\%}$ (gray +) and the bottom 10% value $1/T_1^{-10\%}$ (gray ×) of distributed $1/T_1$, as estimated from $P(1/T_1)$. $1/T_1^{+10\%}$ and $1/T_1^{-10\%}$ keep track with the upper and lower bounds of the distribution in the color contour map in Fig. 3, as expected. But $1/T_1^{+10\%}$ and $1/T_1^{-10\%}$ show qualitatively different behaviors below $T_{\rm charge}$. The faster parts in the sample, represented by $1/T_1^{+10\%}$, begin to increase as soon as charge order sets in. On the other hand, the slower parts in the sample, represented by $1/T_1^{-10\%}$, continue to slow down through $T_{\rm charge}$, as if nothing has happened, until $1/T_1^{-10\%}$ finally begins to increase at $\simeq 30$ K. Note that $1/T_1$ is peaked around 10 K, below which μSR experiments detect static hyperfine fields [28].

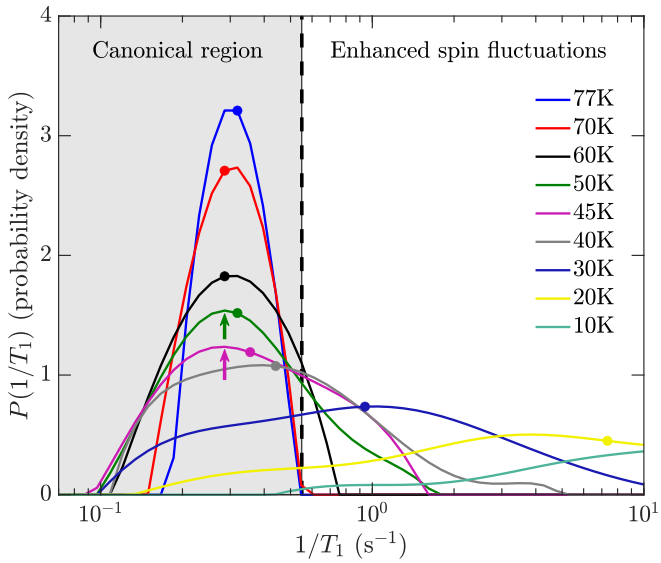

FIG. 5. The closeup view of $P(1/T_1)$ below $T_{charge} \simeq 80$ K. The filled bullets mark $P(1/T_1^{lm})$ at the average value $1/T_1^{lm}$. Although $1/T_1^{lm}$ increases below 60 K, the most likely value of $1/T_1$ represented by the peak location (arrows) continues to slow down. The corresponding shoulder is still recognizable at $1/T_1 \simeq 0.25$ s^{-1} down to $\simeq$20 K. The grey dashed vertical line represents the cutoff value $1/T_1 = 0.55$ s^{-1}. The integral of $P(1/T_1)$ in the shaded region below the cutoff represents the volume fraction of the domains with slow $1/T_1$ expected for canonical superconducting CuO_2 planes, summarized with filled blue bullets in Fig. 6.

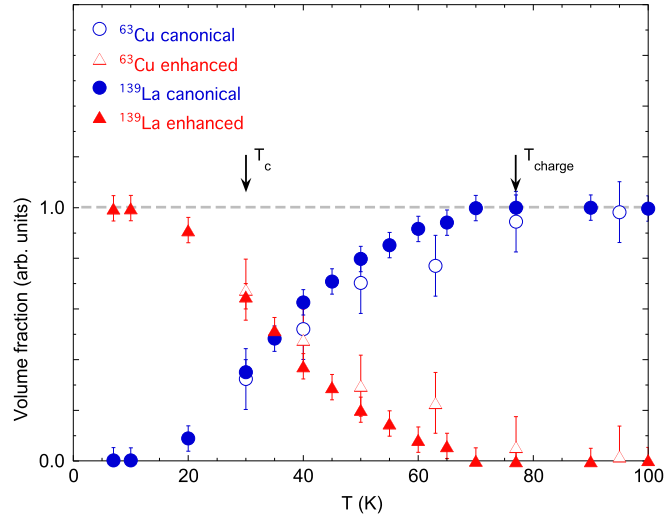

FIG. 6. The volume fraction of the canonically superconducting CuO_2 planes with slow $1/T_1$, as estimated from the integral of $P(1/T_1)$ in the shaded region of Fig. 5 below the cutoff (blue filled bullets), and from the intensity of the normal ^{63}Cu NMR signal (blue open bullets [20]). Also plotted are the volume fraction of the charge-ordered domains with enhanced $1/T_1$ estimated from the integral of $P(1/T_1)$ above the cutoff (red filled triangles) and from the intensity of the winglike ^{63}Cu NMR signals (red open triangles [20]).

The temperature dependence of $1/T_1^{-10\%}$ observed above T_c is very similar to the nondistributed $1/T_1$ observed above T_c for the optimally superconducting phase $La_{1.85}Sr_{0.15}CuO_4$ [42–44]. Combined with the continuing shift of the main peak of $P(1/T_1)$ toward smaller values of $1/T_1$ in the shaded region of Fig. 5, we conclude that a significant volume of the CuO_2 planes continues to behave like the canonical high-T_c superconducting phase even below T_{charge}. It is just that their volume fraction becomes smaller starting from T_{charge}, as evidenced by the suppression of the main peak of $P(1/T_1)$. $1/T_1^{str}$ appears to level off below T_{charge}, merely because it represents the average behavior of different domains with increasing $1/T_1$ and decreasing $1/T_1$. In the case of $La_{1.875}Ba_{0.125}CuO_4$, $1/T_1^{str}$ [6,25,45] as well as $1/T_1^{lm}$ and $1/T_1^{+10\%}$ [25] begin to grow at $T_{charge} \simeq 54$ K, because charge-ordered CuO_2 planes are more homogeneous.

Our conclusion is consistent with the fact that the charge-order correlation length is as short as $\xi \simeq 3$ nm in $La_{1.885}Sr_{0.115}CuO_4$ [3]. In other words, the charge-ordered phase is highly disordered, and the properties of CuO_2 planes are expected to vary with the short length scale ξ. Our conclusion is also corroborated by our earlier ^{63}Cu NMR measurements conducted for the same piece of crystal [20]. A single, narrow ^{63}Cu NMR peak observed above T_{charge} is gradually wiped out, and the lost spectral weight is transferred to a much wider, winglike signal that emerges below T_{charge} underneath the narrow peak. The winglike signals have extremely fast NMR relaxation rates $1/T_1$ and $1/T_2$ and can be detected only with extremely short NMR pulse separation time $\tau \simeq 2$ μs. Since NMR is a local probe, the existence of these two different types of ^{63}Cu NMR signals with drastically different relaxation rates indicates that there are two types of domains below T_{charge} with different magnetic properties. The ^{139}La nuclear spins with slow $1/T_1$ in the shaded region of Fig. 5 and the narrow ^{63}Cu NMR peak with slower relaxation rates originate from the same type of domains that are hardly affected by charge order. The tailed section above the cutoff in Fig. 5 and the winglike ^{63}Cu NMR signals belong to the same domains, in which $1/T_1$ is locally enhanced due to spin freezing triggered by charge order.

We can estimate the volume fraction of the domains affected by charge order using the probability density $P(1/T_1)$, because its integral represents the number of ^{139}La nuclear spins. We introduce a cutoff at $1/T_1 = 0.55$ s^{-1} at the upper end of the distribution of $P(1/T_1)$ observed at 77 K; see the dashed line in Figs. 2 and 5. At 77 K, 100% of the sample volume behaves similarly to canonically superconducting CuO_2 planes, and the entire $P(1/T_1)$ curve is located below the cutoff. Below T_{charge}, spin freezing sets in in charge-ordered domains and $1/T_1$ increases at ^{139}La sites in these domains. As a consequence, a part of the $P(1/T_1)$ curve extends above the cutoff. The integrated area under the $P(1/T_1)$ curve below the cutoff represents the fraction of the canonically behaving domains, whereas the integrated area above the cutoff is from ^{139}La nuclear spins in charge-ordered domains. Needless to say, the summation of the two volume fractions is 100%, because the total integral $\sum_j P(1/T_{1j})\Delta_P = 1$ is normalized to 1.

In Fig. 6, we summarize the temperature dependence of the volume fractions of charge ordered domains with enhanced Cu spin fluctuations (red filled triangles) and domains

unaffected by charge order (blue filled bullets). The agreement with our earlier estimation [20] based on the relative ^{63}Cu NMR intensities of the narrow peak and winglike signals (open symbols) is satisfactory. More importantly, notice that at $T_c = 30$ K a significant fraction of ^{139}La nuclear spins ($\simeq$40%) still relax with $1/T_1$ slower than the cutoff. This means that glassy freezing of Cu spins triggered by charge order hardly affects $\simeq$40% of the CuO_2 planes when superconductivity sets in. This finding is in remarkable contrast with the case of $La_{1.875}Ba_{0.125}CuO_4$ with more strongly suppressed $T_c = 4$ K [21,25]. In $La_{1.875}Ba_{0.125}CuO_4$, the volume fraction affected by charge order quickly grows once charge order sets in at a much lower temperature $T_{\rm charge} \simeq 54$ K, and nearly 100% of the CuO_2 planes are covered by domains with highly enhanced spin fluctuations at 30 K. These contrasting behaviors between $La_{1.885}Sr_{0.115}CuO_4$ and $La_{1.875}Ba_{0.125}CuO_4$ suggest that superconductivity with the higher onset temperature of $T_c = 30$ K survives in the former, probably because nearly a half of the sample volume is unaffected by spin freezing at T_c despite the higher onset of charge order.

IV. SUMMARY AND CONCLUSIONS

We have re-examined the ^{139}La nuclear spin-lattice relaxation process in charge-ordered $La_{1.885}Sr_{0.115}CuO_4$ based on the ILTT$_1$ analysis technique and deduced the histogram of the domain-by-domain distribution of $1/T_1$ in the form of the probability density $P(1/T_1)$. We emphasize that we *deduced* $P(1/T_1)$ by numerically inverting the experimentally observed recovery curve $M(t)$ without assuming the functional form of $M(t)$, such as the stretched exponential [46] or double components [47].

We demonstrated that the main peak of $P(1/T_1)$, associated with the domains without enhanced spin fluctuations, persists even below $T_{\rm charge}$. At the onset of superconductivity at $T_c =$ 30 K, nearly a half of the sample volume remains unaffected by charge order, in agreement with our earlier ^{63}Cu NMR results [20].

Our work reported here and elsewhere [25,26] illustrates the powerful nature of the new ILTT$_1$ analysis techniques applied to disordered quantum materials. The ILT not only probes the average behavior of distributed $1/T_1$ in the form of $1/T_1^{lm}$ ($\simeq 1/T_1^{str}$), but also deduces the histogram of distributed $1/T_1$. The conventional stretched fit analysis of $M(t)$ discards the information about the latter.

ACKNOWLEDGMENTS

We thank S. K. Takahashi and J. Wang for their assistance in NMR data acquisition and analysis. T.I. is financially supported by NSERC. P.M.S. is supported by The Rice University Consortium for Processes in Porous Media. The work at Tohoku was supported by Grant-in-Aid for Scientific Research (A) (Grant No. 16H02125), Japan.

APPENDIX

In this Appendix, we give a brief overview of the ILT analysis, and we refer readers to Supplemental Materials of Ref. [25] for additional mathematical background and the optimization procedures of the ILT, which are based on techniques outlined in Ref. [36].

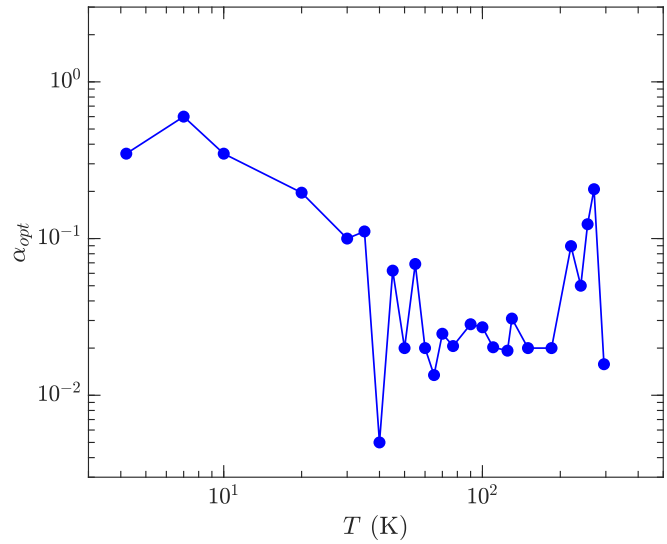

FIG. 7. Temperature dependence of the optimal regularization parameter $\alpha_{\rm opt}$.

The goal of the ILT is to find the solution to the column vector $\mathbf{P}$, i.e., $P(1/T_{1j})$, of length m which minimizes the cost function [38]:

$$\mathbf{P} = \underset{\mathbf{P}\geqslant 0}{\arg\min}\ ||\mathbf{M} - K\,\mathbf{P}||^2 + \alpha||\mathbf{P}||^2 \qquad \text{(A1)}$$

by using non-negative least squares, where $||..||$ is the vector norm. $\mathbf{M}$, i.e., $M(t_i)$, is the column vector of the data of length n. K is the kernel matrix of size $n \times m$ given by

$$K = \left\{K_{ij} = \sum_{k=1}^{4}[1 - 2p_k e^{-q_k t_i/T_{1j}}]\right\}, \qquad \text{(A2)}$$

The first term in Eq. (A1) is the residual between data and fit, and the second term is the Tikhonov regularization factor. α is the scalar regularization parameter (i.e., a smoothing factor) chosen to be large enough to make the solution stable in the presence of noise. The solution $\mathbf{P}(\alpha)$ in Eq. (A1) implicitly depends on α. Choosing $\alpha = 0$ leads to a unique solution $\mathbf{P}(\alpha = 0)$; however the solution is "spiky," where the position and amplitude of the spikes depend on the particular noise realization; this undesirable case is called "under-regularized." In the opposite extreme, choosing a large $\alpha \gg 10$ oversmooths the solution $\mathbf{P}(\alpha \gg 10)$; this undesirable case is so called "over-regularized."

The optimal regularization parameter $\alpha_{\rm opt}$ is determined using the Bulter-Reeds-Dawson (BRD) condition [38], together with the "heel" condition [37]. The BRD condition corresponds to when the residual between data and fit obtains the statistical noise floor. The heel condition corresponds to when systematic errors in the experimental data dominate the residual between data and fit. Systematic errors occur due to hardware limitations which are only apparent at high signal-to-noise ratio (SNR), or the kernel K may not be exact due to the presence of quadrupole relaxation. The results are plotted in Fig. 7, which indicate that $\alpha_{\rm opt}$ increases somewhat

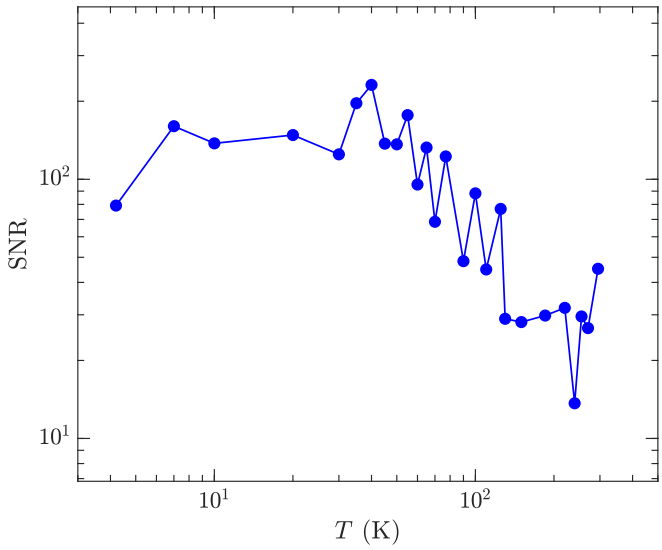

FIG. 8. Temperature dependence the signal-to-noise ratio (SNR).

at lower temperatures. This is a result of the heel condition being met more often than the BRD condition.

As shown in Fig. 8, the SNR increases from SNR $\simeq$ 50 to SNR $\simeq$ 200 with decreasing temperature. The Supplemental Materials of Ref. [25] show an example of a forward model as a function of SNR using synthetic noise. The forward model indicates that at SNR $=$ 50, the peaks are distinguishable provided they are a half-decade apart in $1/T_1$. As such, a half-decade in $1/T_1$ may loosely be considered as the ILT "resolution" at SNR $=$ 50, although this is only semiquantitative. The resolution can in principle improve with increasing SNR. The temperature dependence of the SNR in Fig. 8 indicates that a resolution of less than a half-decade in $1/T_1$ is possible $\lesssim$100 K, provided the BRD condition for $\alpha_{\rm opt}$ is met rather than the heel condition. If the heel condition is met, then increasing the SNR does not necessarily improve the resolution.

Regarding uncertainties in the optimal solution **P**, we note that there are no uncertainties or "error bars" associated with each bin j of the $P(1/T_{1j})$ distribution. Instead, uncertainties in the moments of **P** such as $1/T_1^{lm}$ (log mean) or σ_e (log standard deviation) can be quantified. Furthermore, uncertainties in the total area of **P** [i.e., $\sum_{j=1}^{m} P(1/T_{1j}) = M_0$] and the partial area of **P** below [i.e., $\sum_{j=1}^{m,cut} P(1/T_{1j})$] or above [i.e., $\sum_{j=m,cut}^{m} P(1/T_{1j})$] a certain a cutoff $(1/T_1)_{cut}$ can also be quantified. Details of how to quantify these uncertainties can be found in Refs. [40,48], which are beyond the scope of this report.

[1] T. P. Croft, C. Lester, M. S. Senn, A. Bombardi, and S. M. Hayden, Phys. Rev. B **89**, 224513 (2014).

[2] V. Thampy, M. P. M. Dean, N. B. Christensen, L. Steinke, Z. Islam, M. Oda, M. Ido, N. Momono, S. B. Wilkins, and J. P. Hill, Phys. Rev. B **90**, 100510(R) (2014).

[3] J. Wen, H. Huang, S. J. Lee, H. Jang, J. Knight, Y. S. Lee, M. Fujita, K. M. Suzuki, S. Asano, S. A. Kivelson, C. C. Kao, and J.-S. Lee, Nat. Commun. **10**, 3269 (2019).

[4] A. W. Hunt, P. M. Singer, K. R. Thurber, and T. Imai, Phys. Rev. Lett. **82**, 4300 (1999).

[5] P. M. Singer, A. W. Hunt, A. F. Cederström, and T. Imai, Phys. Rev. B **60**, 15345 (1999).

[6] A. W. Hunt, P. M. Singer, A. F. Cederström, and T. Imai, Phys. Rev. B **64**, 134525 (2001).

[7] We initially overestimated the onset temperature of charge order below $x \simeq 1/8$ in Refs. [4] and [5] due to the charge localization effect. See Fig. 18 and related discussions in Ref. [6] for details.

[8] J. M. Tranquada, B. J. Sternlieb, J. D. Axe, Y. Nakamura, and S. Uchida, Nature (London) **375**, 561 (1995).

[9] M. Fujita, H. Goka, K. Yamada, J. M. Tranquada, and L. P. Regnault, Phys. Rev. B **70**, 104517 (2004).

[10] J. Fink, V. Soltwisch, J. Geck, E. Schierle, E. Weschke, and B. Büchner, Phys. Rev. B **83**, 092503 (2011).

[11] T. Wu, H. Mayaffre, S. Krämer, M. Horvatić, C. Berthier, W. N. Hardy, R. Liang, D. A. Bonn, and M.-H. Julien, Nature (London) **477**, 191 (2011).

[12] A. J. Achkar, R. Sutarto, X. Mao, F. He, A. Frano, S. Blanco-Canosa, M. Le Tacon, G. Ghiringhelli, L. Braicovich, M. Minola, M. Moretti Sala, C. Mazzoli, R. Liang, D. A. Bonn, W. N. Hardy, B. Keimer, G. A. Sawatzky, and D. G. Hawthorn, Phys. Rev. Lett. **109**, 167001 (2012).

[13] E. Blackburn, J. Chang, M. Hücker, A. T. Holmes, N. B. Christensen, R. Liang, D. A. Bonn, W. N. Hardy, U. Rütt, O. Gutowski, M. v. Zimmermann, E. M. Forgan, and S. M. Hayden, Phys. Rev. Lett. **110**, 137004 (2013).

[14] S. Blanco-Canosa, A. Frano, T. Loew, Y. Lu, J. Porras, G. Ghiringhelli, M. Minola, C. Mazzoli, L. Braicovich, E. Schierle, E. Weschke, M. Le Tacon, and B. Keimer, Phys. Rev. Lett. **110**, 187001 (2013).

[15] A. J. Achkar, X. Mao, C. McMahon, R. Sutarto, F. He, R. Liang, D. A. Bonn, W. N. Hardy, and D. G. Hawthorn, Phys. Rev. Lett. **113**, 107002 (2014).

[16] M. Hücker, N. B. Christensen, A. T. Holmes, E. Blackburn, E. M. Forgan, R. Liang, D. A. Bonn, W. N. Hardy, O. Gutowski, M. v. Zimmermann, S. M. Hayden, and J. Chang, Phys. Rev. B **90**, 054514 (2014).

[17] S. Blanco-Canosa, A. Frano, E. Schierle, J. Porras, T. Loew, M. Minola, M. Bluschke, E. Weschke, B. Keimer, and M. Le Tacon, Phys. Rev. B **90**, 054513 (2014).

[18] E. H. da Silva Neto, P. Aynajian, A. Frano, R. Comin, E. Schierle, E. Weschke, A. Gyenis, J. Wen, J. Schneeloch, Z. Xu, S. Ono, G. Gu, M. Le Tacon, and A. Yazdani, Science **343**, 393 (2014).

[19] J. M. Tranquada, N. Ichikawa, and S. Uchida, Phys. Rev. B **59**, 14712 (1999).

[20] T. Imai, S. K. Takahashi, A. Arsenault, A. W. Acton, D. Lee, W. He, Y. S. Lee, and M. Fujita, Phys. Rev. B **96**, 224508 (2017).

[21] T. Imai, A. Arsenault, P. M. Singer, and M. Fujita (unpublished).

[22] A. Arsenault, S. K. Takahashi, T. Imai, W. He, Y. S. Lee, and M. Fujita, Phys. Rev. B **97**, 064511 (2018).

[23] P. M. Singer, D. Asthagiri, Z. Chen, A. Valiya Parambathu, G. J. Hirasaki, and W. G. Chapman, J. Chem. Phys. **148**, 164507 (2018).
[24] P. M. Singer, D. Asthagiri, W. G. Chapman, and G. J. Hirasaki, J. Chem. Phys. **148**, 204504 (2018).
[25] P. M. Singer, A. Arsenault, T. Imai, and M. Fujita, Phys. Rev. B **101**, 174508 (2020).
[26] S. K. Takahashi, J. Wang, A. Arsenault, T. Imai, M. Abramchuk, F. Tafti, and P. M. Singer, Phys. Rev. X **9**, 031047 (2019).
[27] H. Kimura, K. Hirota, H. Matsushita, K. Yamada, Y. Endoh, S.-H. Lee, C. F. Majkrzak, R. Erwin, G. Shirane, M. Greven, Y. S. Lee, M. A. Kastner, and R. J. Birgeneau, Phys. Rev. B **59**, 6517 (1999).
[28] K. Kumagai, K. Kawano, I. Watanabe, K. Nishiyama, and K. Nagamine, Hyperfine Interact. **86**, 473 (1994).
[29] A. T. Savici, Y. Fudamoto, I. M. Gat, T. Ito, M. I. Larkin, Y. J. Uemura, G. M. Luke, K. M. Kojima, Y. S. Lee, M. A. Kastner, R. J. Birgeneau, and K. Yamada, Phys. Rev. B **66**, 014524 (2002).
[30] E. R. Andrew and D. P. Tunstall, Proc. Phys. Soc. **78**, 1 (1961).
[31] A. Narath, Phys. Rev. **162**, 320 (1967).
[32] P. Thayamballi and D. Hone, Phys. Rev. B **21**, 1766 (1980).
[33] M. Itoh, H. Yasuoka, A. R. King, and V. Jaccarino, J. Phys. Soc. Jpn. **55**, 964 (1986).
[34] C. P. Lindsey and G. D. Patterson, J. Chem. Phys. **73**, 3348 (1980).
[35] D. C. Johnston, S.-H. Baek, X. Zong, F. Borsa, J. Schmalian, and S. Kondo, Phys. Rev. Lett. **95**, 176408 (2005).
[36] L. Venkataramanan, Y. Q. Song, and M. D. Hürlimann, IEEE Trans. Signal Proc. **50**, 1017 (2002).
[37] Y. Q. Song, L. Venkataramanan, M. D. Hürlimann, M. Flaum, P. Frulla, and C. Straley, J. Magn. Res. **154**, 261 (2002).
[38] J. P. Butler, J. A. Reeds, and S. V. Dawson, SIAM J. Numer. Anal. **18**, 381 (1981).
[39] E. Chouzenoux, S. Moussaoui, J. Idier, and F. Mariette, IEEE Trans. Sig. Process. **58** (12), 6040 (2010).
[40] M. Prange and Y.-Q. Song, J. Magn. Reson. **196**, 54 (2009).
[41] See Supplemental Material of [25] at http://link.aps.org/supplemental/10.1103/PhysRevB.101.184505 for more technical details about ILT.
[42] T. Kobayashi, S. Wada, Y. Kitaoka, and K. Asayama, J. Phys. Soc. Jpn. **58**, 2662 (1989).
[43] K. Yoshimura, T. Uemura, M. Kato, T. Shibata, K. Kosuge, T. Imai, and H. Yasuoka, Springer Proc. Phys. **60**, 405 (1992).
[44] S.-H. Baek, A. Erb, and B. Büchner, Phys. Rev. B **96**, 094519 (2017).
[45] S.-H. Baek, Y. Utz, M. Hücker, G. D. Gu, B. Büchner, and H.-J. Grafe, Phys. Rev. B **92**, 155144 (2015).
[46] The single-component stretched fit of $M(t)$ is actually based on an implicit assumption that $P(1/T_1)$ has a peculiar form of distribution, which is different from $P(1/T_1)$ observed in the present case. See Fig. 5 and related discussions in Ref. [35] for details.
[47] The slow and fast components of $1/T_1$ estimated from the double component fit of $M(t)$ in our earlier work [22] agree with $1/T_1^{-10\%}$ and $1/T_1^{+10\%}$ fairly well. In essence, our two-component analysis of $1/T_1$ approximated the continuous distribution of $1/T_1$ with two distinct peaks located near the lower and upper ends of $P(1/T_1)$. Also note that two distinct peaks of $P(1/T_1)$ are indeed present for Cu_2IrO_3, and the $1/T_1$ values estimated from the two-component fit agree well with the peak locations [26]. On the other hand, the two-component fit is stable only around $\simeq$50 K for $La_{1.875}Ba_{0.125}CuO_4$, because $P(1/T_1)$ exhibits more symmetrical shapes.
[48] L. Venkataramanan, F. K. Gruber, T. M. Habashy, and D. E. Freed, J. Magn. Reson. **206**, 20 (2010).